Journal of Physical Chemistry and Functional Materials

Home Page of Journal: https://dergipark.org.tr/jphcfum

Synthesis and Characterization of CeO_2 samples doped with Bi

Tankut Ates [a,*], Serhat Keser [b], Niyazi Bulut [c], Omer Kaygili [c]

[a] *Department of Engineering Basic Sciences, Faculty of Engineering and Natural Sciences, Malatya Turgut Özal University, Battalgazi, Malatya, Türkiye*

[b] *Department of Chemical Technology, EOSB Higher Vocational School, Firat University, Elazig, Türkiye*

[c] *Department of Physics, Faculty of Science, Firat University, Elazig, Türkiye*

* *Corresponding author: E-mail: tankut.ates@ozal.edu.tr*

ABSTRACT

In the present paper, the effects of bismuth (Bi) on the structural properties and morphology of cerium dioxide (CeO_2) structure. One un-doped and four Bi-doped CeO_2 samples were manufactured and characterized by X-ray diffraction (XRD), Fourier transform infrared (FTIR), and scanning electron microscopy (SEM) techniques. The XRD and FTIR results confirmed the formation of the CeO_2 with the cubic crystal structure. Any secondary phase was not observed with the addition of Bi. The crystallite size for each sample is in the nanometer scale. The crystallinity, average crystallite size and lattice parameter were affected by Bi-content. The amount of the additive of Bi affected the morphology of the as-produced samples.

ARTICLE INFO

Keywords:
Bismuth,
Cerium dioxide,
X-ray diffraction,
Morphology

Received: 2024-09-13
Accepted: 2024-10-19
ISSN: 2651-3080
DOI: **10.54565/jphcfum.1549331**

1. INTRODUCTION

Cerium (Ce) is a member of the lanthanide series with an atomic number of 58, classified as a rare earth metal. Among lanthanide oxides, cerium oxide is the most abundant, low-cost, environmentally friendly, and highly reactive element. It also serves as an electropositive ion in 4+ and 3+ oxidation states and functions as an n-type semiconductor [1-4]. In the 4+ oxidation state, Ce^{4+} has an electronic configuration of [Xe]4f0, making it more stable than Ce^{3+} [Xe]4f1 due to its empty f-orbital. Cerium exists as cerium dioxide (Cerium(IV) Oxide) (CeO_2) in the 4+ oxidation state and as cerium sesquioxide (Cerium(III) Oxide) (Ce_2O_3) in the 3+ oxidation state [1]. The ease of interconversion between the 3+ and 4+ oxidation states of cerium makes it a desirable material in many fields. The crystal structure of cerium oxide (CeO_2), one of the most stable oxides, is a face-centered cubic fluorite with a space group of Fm3m [1,4]. In this crystal structure, cerium ions occupy the alternate cube centers of a simple cubic lattice, with each metal ion surrounded by eight oxygen atoms [1]. Additionally, CeO_2 is a semiconductor with an electronic band gap in the range of 3.4-3.5 eV, a wide optical band gap of 5.5 eV, and a dielectric constant value of $\varepsilon = 26$ [4].

Cerium oxide (CeO_2) has long been a material of interest in various fields due to its superior properties. Notably, its redox behavior and oxygen storage capabilities, owing to the oxidation between Ce^{3+} and Ce^{4+}, make it critically important in applications such as solid oxide fuel cells and as a support for three-way catalysts in pollution control [1,5,3,6]. It also exhibits properties essential for use as a biomaterial component, such as antibacterial activities, antioxidant, antimicrobial, angiogenic potential, and anti-inflammatory properties [5,7,3].

Moreover, CeO_2 possesses positive attributes like gas sensitivity, ultraviolet absorption ability, low phonon energy, photocatalytic activities, photoluminescence (PL), contribution to wound healing processes, thermal stability, high efficiency, and high chemical stability [7,5,8,4]. These features make CeO_2 materials highly desirable for a wide range of applications, including gas sensors, optical applications, photocatalysts, LED technologies, therapeutic tools, multimodal biological imaging, drug

delivery, biological labeling, water purification, UV-resistant composite materials, electrode fabrication in electrolytes, and chemical-mechanical polishing for microelectronics [3,7,8,1,6].

To date, various synthetic routes have been developed for the preparation of CeO_2-based mixed oxides, including co-precipitation, high-temperature calcinations, high-energy mechanical milling, surfactant-assisted approaches, microemulsion, sol-gel techniques, and chemical impregnation. Synthesizing CeO_2-based mixed oxides with well-controlled morphologies is desirable for exploring morphology-property relationships and expanding their applications [6]. For example, various cerium morphologies such as nanowires, nanorods, nanospheres, and nanocubes have been synthesized [9].

In different application fields, it is necessary to introduce different atoms into the crystal structure to enhance the activity and efficiency of CeO_2. To date, the properties of various cerium oxide composites have been investigated by adding divalent, trivalent, and pentavalent cations into the crystal structure of CeO_2. These cations can be used in single or multiple combinations [3]. The elements, including Co [10], Y [11], Er [12], Gd [13], Cr [14], Sm [15], Zr [16], Fe [17], Cu [18], Pd, Au [19], Ag [4], La [20], Pr [21], and Ca [22], have been used for a dopant for the CeO_2. Tian et al. [23] investigated the conversion of carbon dioxide to formic acid on Bi-doped CeO_2 under tensile and compressive stress and demonstrated that it serves as a model with excellent product selectivity, offering the best catalytic performance for formic acid. Santra et al. [24] found that the addition of Bi dopants to the CeO_2 structure results in the formation of oxygen vacancies, thereby establishing an alternative and simple methodology for developing oxidation catalysts of industrial interest. Pütz et al. [25] reported a significant enhancement in the catalytic activity of nanoceria as a result of Bi3+ substitution.

In the present study, the effects of increasing Bi-content, from 0.35 at.% to 1.40 at.%, on the structural properties of the CeO_2 samples synthesized by a wet chemical route were investigated.

2. MATERIAL AND METHOD

Cerium (III) nitrate hexahydrate ($Ce(NO_3)_3{\bullet}6H_2O$), bismuth(III) nitrate pentahydrate ($Bi(NO_3)_3{\bullet}5H_2O$), and ammonia (NH_3) purchased from Sigma-Aldrich were used in the synthesis of the un-doped and Bi-doped CeO_2 samples. As a solvent, the distilled water was used. A solution, having a total volume of 100 mL, of (25.0000-x) mmol of $Ce(NO_3)_3{\bullet}6H_2O$ and x mmol of $Bi(NO_3)_3{\bullet}5H_2O$ was prepared for each sample. Where x value was selected as 0, 0.0875, 0.1750, 0.2625 and 0.3500. The pH was adjusted to the value of 10.0 by using NH_3 solution. Each solution was stirred in a magnetic stirrer at 65 °C for 5 h, and then was dried in an oven at 120 °C for 39 h. The as-obtained dry samples were heated in an electric furnace at 900 °C for 3 h. The un-doped and Bi-doped CeO_2 at different amounts (e.g., 0.35, 0.70, 1.05 and 1.40at.%) samples were produced.

The characterization of the as-manufactured oxides was performed by X-ray diffraction (XRD), Fourier transform infrared (FTIR) and scanning electron microscopy analyses. The XRD patterns were collected by a Bruker D8 Advance diffractometer within 2θ range from 20° to 80° with a step of 0.02°. The FTIR spectra were recorded by a Perkin Elmer Spectrum One spectrophotometer using the KBr method. An FEI Quanta 450 FEG scanning electron microscope was used to investigate the morphology of the samples.

3. RESULTS AND DISCUSSIONS

3.1. XRD results

Fig. 1 illustrates the XRD patterns of the as-produced samples. All the patterns match with the cerium oxide (CeO_2, JCPDS pdf no: 65-2975) with the cubic crystal structure [26]. The peaks located about at the 2θ positions of 28.70°, 33.25°, 47.65°, 56.50°, 59.20°, 69.60°, 76.85° and 79.20° are related to the planes of the (111), (200), (220), (311), (222), (400), (331) and (420), respectively. There is no any peak assigned to the impurity (e.g., Bi and its oxide form) in these patterns. The fact that the distribution of a single phase of the CeO_2 was detected for each sample and no secondary phase was observed with the addition of Bi, indicating high purity for the obtained samples [4].

The average crystallite size (D) values were computed using the following Scherrer equation [4]:

$$D = \frac{0.9\lambda}{\beta \cos\theta} \quad (1)$$

where the θ, β and λ are known as the Bragg's angle, full width at half-maximum and wavelength of incident X-rays, respectively. For the calculation of the lattice parameter (a=b=c) and unit cell volume (V) for the cubic crystal structure, the following relations were used:

$$a = d\sqrt{h^2 + k^2 + l^2} \quad (2)$$

$$V = a^3 \quad (3)$$

where d is the interplanar distance.

The expression used for estimating the crystallinity percent (X_C%) for each sample is given as follow:

$$X_C\% = \frac{\sum A_C}{\sum A_C + \sum A_A} \times 100 \quad (4)$$

here the $\sum A_C$ and $\sum A_A$ point out the total areas under crystal and amorphous peaks, respectively.

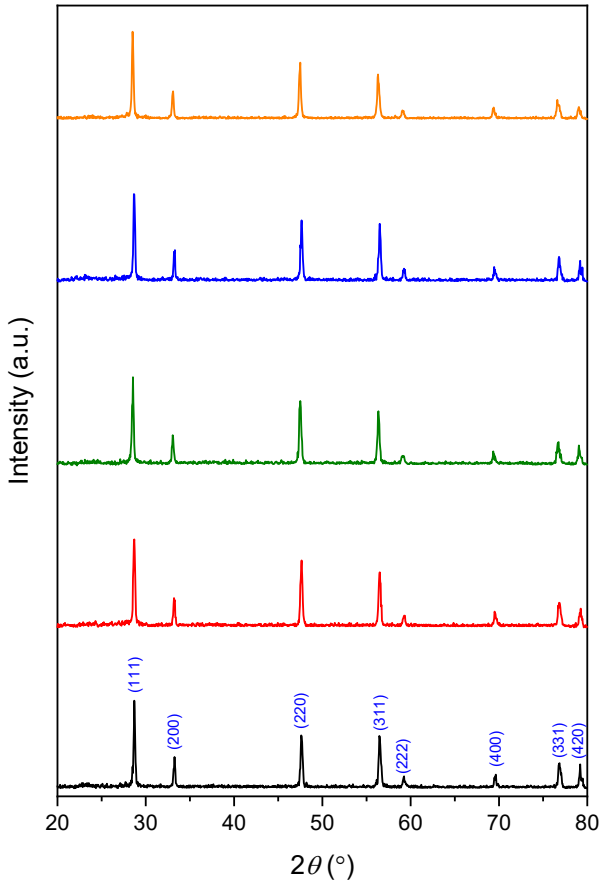

Fig. 1. XRD patterns of the as-manufactured samples

As can be seen from the results given in Table 1, the lattice parameters of the CeO_2 change with the increase in Bi content. Bi content affects the crystallite size and crystallinity, but this effect is irregular. Since the crystallite size for each sample is in the nanometer scale, it can be commented that the prepared samples can be used in biological applications [4].

Table 1. The calculated values of the average crystallite size, crystallinity percent, lattice parameter and unit cell volume of the samples

	D (nm)	*Xc%*	*a* (nm)	*V* $(nm)^3$
CeO_2	35.60	93.7	0.5402	0.1576
0.35Bi-CeO_2	32.22	93.1	0.5397	0.1572
0.70Bi-CeO_2	34.17	93.5	0.5414	0.1587
1.05Bi-CeO_2	36.42	93.2	0.5409	0.1583
1.40Bi-CeO_2	35.47	94.3	0.5417	0.1590

3.2. FTIR analysis

The FTIR results shown in Fig. 2 reveal the functional groups found in the samples. In these spectra, the bands associated with different bonds were detected in the spectral interval of 4000-400 cm^{-1}. The band observed at 716 cm^{-1} is thought to be associated with the characteristic vibration of the Ce-O bond, while the band at 1063 cm^{-1} is believed to be related to the vibration of the C-O bond [4]. The band at 1403 cm^{-1} represents the vibrational mode of N-O stretching, which is attributed to the presence of nitrate [26]. The band at 1749 cm^{-1} can be assigned to the C=O stretching modes [27]. Additionally, a band observed at 2901 and 2980 cm^{-1} can be attributed to the vibrational modes of C-H stretching [4,27]. Finally, the weak band observed at 3674 cm^{-1} may be due to the O-H stretching of water molecules [4].

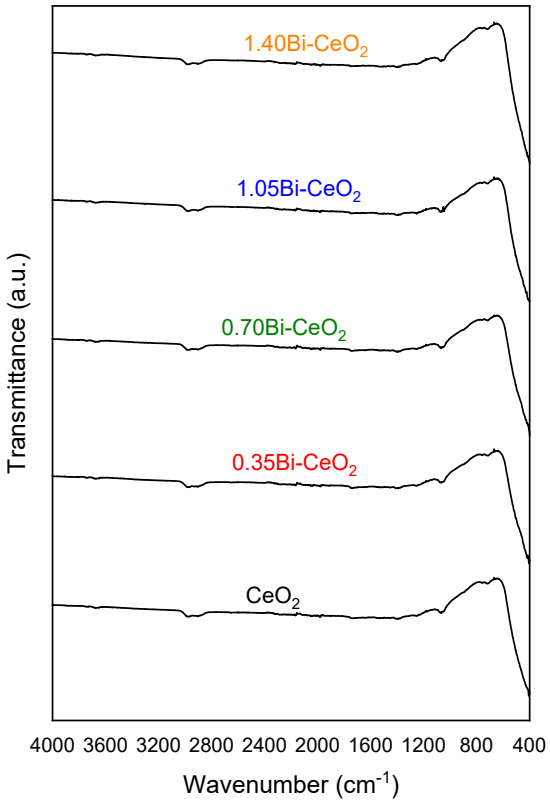

Fig. 2. FTIR spectrum for each sample

3.3. Morphological investigation by SEM and EDX

The SEM images and energy dispersed X-ray (EDX) analysis reports of the samples are shown in Fig. 3. As can be seen from these images, the morphology of the CeO_2 structure is affected by Bi-content. The EDX spectra verify that all the Bi-doped CeO_2 samples are composed of Ce, O and Bi, and the un-doped one is composed Ce and O. The increasing amount of Bi was detected for the samples having higher Bi-contents. The morphology is composed

of the stacked nano-sized particles and is affected by the amount of Bi.

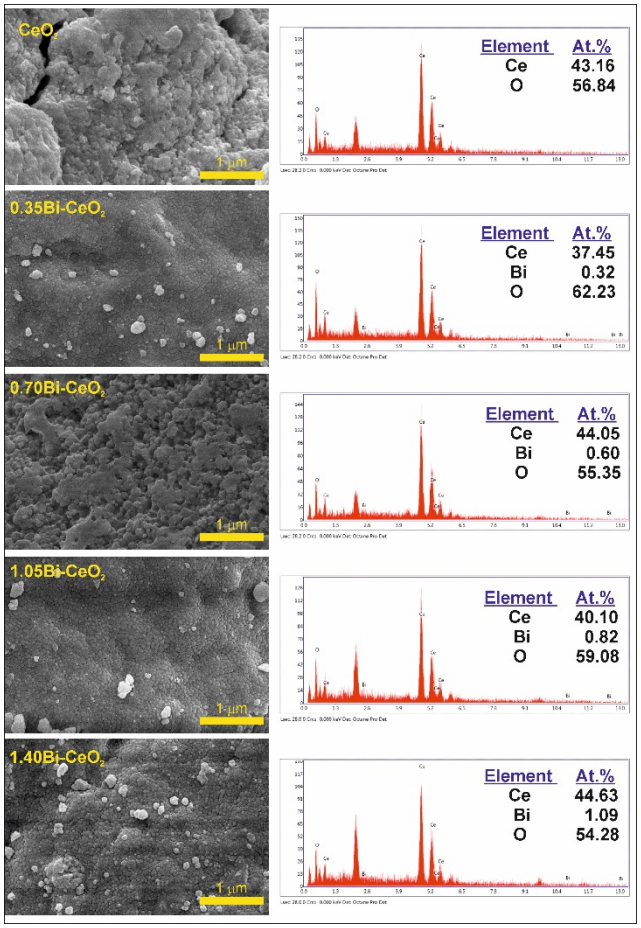

Fig. 3. SEM and EDX results of the samples

4. DISCUSSION

The un-doped and Bi-doped CeO_2 nanostructures were successfully synthesized using a wet chemical method. The effects of Bi doping on the CeO_2 structure were determined through XRD, FTIR, SEM, and EDX analyses. XRD analyses revealed that a single-phase CeO_2 with a cubic crystal structure formed in all samples, and the phase structure was not influenced by the Bi content. It was determined that the incorporation of Bi into the CeO_2 structure at different concentrations affected the lattice parameters, crystallite size, and crystallinity, though this effect caused a non-gradual change. SEM images indicated that the morphology of the CeO_2 structure was influenced by the Bi content, and EDX results confirmed the purity of the samples. The morphology is composed of the stacked nano-sized particles and is affected by the amount of Bi.

Competing interests

The authors declare that they have no competing interests.

Acknowledgements

N.B is grateful for support from the Poland National Science Foundation (NAWA) Grand and also the COST actions CA21101 and CA22148. This work was supported by the Management Unit of Scientific Research Projects of Firat University (FUBAP) (Project Number: FF.24.03 and ADEP.24.09).

REFERENCES

[1] K. Hudda, B. Rathee, M. Wati, S. Ranga and R. TyagI. Some Applications of CeO_2 Nanoparticles. Oriental Journal of Chemistry. 2023;39(3):684-693. http://dx.doi.org/10.13005/ojc/390319.

[2] Z. Yuan, T. Cao, M. Deng, J. Ma, S. Geng, C. Yang, Y. Ren, M. Yao, F. Liu and X. Wang. Unveiling the CeO_2 morphology effect in Pd-CeO_2/C heterostructures catalysts for formic acid dehydrogenation. Fuel. 2023;346:128333. https://doi.org/10.1016/j.fuel.2023.128333.

[3] R. Kırkgeçit, H.Ö. Torun, F.K. Dokan and E. Öztürk. Investigation of photochemical properties of La-Er/CeO_2 and La-Y/CeO_2 composites. Journal of Photochemistry and Photobiology A: Chemistry. 2022;423:113602. https://doi.org/10.1016/j.jphotochem.2021.113602.

[4] T. Ates. Synthesis and characterization of Ag-doped CeO_2 powders. Journal of the Australian Ceramic Society. 2021;57(2):615-623. https://doi.org/10.1007/s41779-021-00565-6.

[5] M.Ç. Yurtsever and G. Güldağ. TiO_2, CeO_2, and TiO_2–CeO_2 nanoparticles incorporated 2.5 D chitosan hydrogels: Gelation behavior and cytocompatibility. Journal of the Mechanical Behavior of Biomedical Materials. 2023;146:106088. https://doi.org/10.1016/j.jmbbm.2023.106088.

[6] Q. Fang and X. Liang. CeO_2–Al_2O_3, CeO_2–SiO_2, CeO_2–TiO_2 core-shell spheres: formation mechanisms and UV absorption. RSC Advances. 2012;2(12):5370-5375. https://doi.org/10.1039/C2RA01331B.

[7] M.S. Pudovkin, O.A. Morozov, S.L. Korableva, R.M. Rakhmatullin, V.V. Semashko, A.K. Ginkel, A.A. Rodionov and A.G. Kiiamov. EPR and optical study of erbium-doped CeO_2 and CeO_2/CeF_3 nanoparticles. Ceramics International. 2024;50(6):9263-9269. https://doi.org/10.1016/j.ceramint.2023.12.242.

[8] K.Q. Liu, C.B. Wu and W.Q. Kang. Preparation of CeO_2-PVA composite film based on in-situ generation of nano CeO_2 particles. Optical Materials. 2024;148:114840. https://doi.org/10.1016/j.optmat.2024.114840.

[9] S. Paydar, B. Zhu, J. Shi, N. Akbar, Q.A. Islam, S. Yun, A. Muhammad, M.H. Paydar and Y. Wu. Surfacial proton conducting CeO_2 nanosheets. Ceramics International. 2023;49(6):9138-9146. https://doi.org/10.1016/j.ceramint.2022.11.073.

[10] S.B. Bošković, D.R. Djurović, S.P. Zec, B.Z. Matović, M. Zinkevich and F. Aldinger. Doped and Co-doped CeO_2: Preparation and properties. Ceramics international. 2008;34(8):2001-2006. https://doi.org/10.1016/j.ceramint.2007.07.036.

[11] F.A. Berutti, A.K. Alves, C.P. Bergmann, F.J. Clemens and T. Graule. Synthesis of CeO_2 and Y_2O_3-doped CeO_2 composite fibers by electrospinning. Particulate Science and Technology. 2009;27(3):203-209. https://doi.org/10.1080/02726350902921681.

[12] M.S. Pudovkin, O.A. Morozov, S.L. Korableva, R.M. Rakhmatullin, V.V. Semashko, A.K. Ginkel, A.A. Rodionov and A.G. Kiiamov. EPR and optical study of erbium-doped CeO_2 and CeO_2/CeF_3 nanoparticles. Ceramics International. 2024;50(6):9263-9269. https://doi.org/10.1016/j.ceramint.2023.12.242.

[13] Y.G. Kim and S.B. Kim. Microwave Sintering of Gd-Doped CeO_2 Powder. Journal of the Korean Ceramic Society. 2007;44(3):182. https://doi.org/10.4191/kcers.2007.44.3.182.

[14] S. Phokha, D. Prabhakaran, A. Boothroyd, S. Pinitsoontorn and S. Maensiri. Ferromagnetic induced in Cr-doped CeO_2 particles. Microelectronic engineering. 2014;126:93-98. https://doi.org/10.1016/j.mee.2014.06.028.

[15] S. Ramesh. Transport properties of Sm doped CeO_2 ceramics. Processing and Application of Ceramics. 2021;15(4):366-373. https://doi.org/10.2298/PAC2104366R.

[16] B. He, Y. Li, H.Y. Zhang, D.L. Wu, L.H. Liang and H. Wei. Phase transformation of ZrO_2 doped with CeO_2. Rare Metals. 2018;37:66-71. https://doi.org/10.1007/s12598-015-0552-z.

[17] N. Paunović, Z.V. Popović and Z.D. Dohčević-Mitrović. Superparamagnetism in iron-doped CeO2− y nanocrystals. Journal of Physics: Condensed Matter. 2012;24(45):456001. https://doi.org/10.1088/0953-8984/24/45/456001.

[18] P. Slusser, D. Kumar and A. Tiwari. Unexpected magnetic behavior of Cu-doped CeO_2. Applied Physics Letters. 2010;96(14):142506. https://doi.org/10.1063/1.3383238.

[19] Y. Park, S.K. Kim, D. Pradhan and Y. Sohn. Thermal H 2-treatment effects on CO/CO_2 conversion over Pd-doped CeO_2 comparison with Au and Ag-doped CeO_2. Reaction Kinetics, Mechanisms and Catalysis. 2014;113:85-100. https://doi.org/10.1007/s11144-014-0757-4.

[20] P.R. Keating, D.O. Scanlon and G.W. Watson. The nature of oxygen states on the surfaces of CeO_2 and La-doped CeO_2. Chemical Physics Letters. 2014;608:239-243. https://doi.org/10.1016/j.cplett.2014.05.094.

[21] V. Sharma, K. Eberhardt, R. Sharma and P. Crozier. Nano-scale compositional heterogeneity in pr-doped Ceo2. Microscopy and Microanalysis. 2009;15(S2):700-701. https://doi.org/10.1017/S1431927609098705.

[22] H. Yamamura, S. Takeda and K. Kakinuma. Dielectric relaxations in the Ca-doped CeO_2 system. Journal of the Ceramic Society of Japan. 2007;115(1344):471-474. https://doi.org/10.2109/jcersj2.115.471.

[23] A. Tian, Z. Mei, L. Wang, G. Liu, Z. Liu, G. Kong, W. Tang and C. Liu. Improved photocatalytic carbon dioxide reduction over Bi-doped CeO_2 by strain engineering. Sustainable Energy & Fuels. 2024;8(7):1405-1411. https://doi.org/10.1039/D3SE01680C.

[24] C. Santra, A. Auroux and B. Chowdhury. Bi doped CeO_2 oxide supported gold nanoparticle catalysts for the aerobic oxidation of alcohols. RSC advances. 2016;6(51):45330-45342. https://doi.org/10.1039/C6RA05216A.

[25] E. Pütz, I. Tutzschky, H. Frerichs and W. Tremel. In situ generation of H_2O_2 using CaO_2 as peroxide storage depot for haloperoxidase mimicry with surface-tailored Bi-doped mesoporous CeO_2 nanozymes. Nanoscale. 2023;15(11):5209-5218. https://doi.org/10.1039/D2NR02575B.

[26] M. Romero-Saez, R. Suresh, N. Benito, S. Rajendran, F. Gracia, C. Navas-Cárdenas, A.K. Priya and M. Soto-Moscoso. Defective Ce^{3+} associated CeO_2 nanoleaves for enhanced CO oxidation. Fuel. 2022;315:122822. https://doi.org/10.1016/j.fuel.2021.122822.

[26] G. Murugadoss, J. Ma, X. Ning and M.R. Kumar. Selective metal ions doped CeO_2 nanoparticles for excellent photocatalytic activity under sun light and supercapacitor application. Inorganic Chemistry Communications. 2019;109:107577. https://doi.org/10.1016/j.inoche.2019.107577.

[27] T. Umehara, M. Hagiwara and S. Fujihara. Synthesis of hollow and aggregated CeO_2: Sm^{3+} microspheres and their redox-responsive luminescence. Journal of Alloys and Compounds. 2019;787:1074-1081. https://doi.org/10.1016/j.jallcom.2019.02.129.